

Guidelines for understanding cubic manganese-rich Heusler compounds

Lukas Wollmann,¹ Stanislav Chadov,¹ Jürgen Kübler,² Claudia Felser¹

¹*Max-Planck-Institut für Chemische Physik fester Stoffe,
Nöthnitzer Strasse 40, 01187 Dresden, Germany and*

²*Institut für Festkörperphysik, Technische Universität Darmstadt, 64289 Darmstadt, Germany*

Manganese-rich Heusler compounds are attracting much interest in the context of spin transfer torque and rare-earth free hard magnets. Here we give a comprehensive overview of the magnetic properties of non-centrosymmetric cubic Mn₂-based Heusler materials, which are characterized by an antiparallel coupling of magnetic moments on Mn atoms. Such a ferrimagnetic order leads to the emergence of new properties that are absent in ferromagnetic centrosymmetric Heusler structures. In terms of the band structure calculations, we explain the formation of this magnetic order and the Curie temperatures. This overview is intended to establish guidelines for a basic understanding of magnetism in Mn₂-based Heusler compounds.

PACS numbers: 75.50.Gg, 71.15.Nc, 75.10.Lp, 75.30.Et

I. INTRODUCTION

Heusler compounds became objects of interest as a class of materials with peculiar transport and magneto-optical properties with the prediction of half-metallicity (gapping in one spin channel) in NiMnSb and Co₂MnSn^{1,2} in 1983. The whole family of Co₂YZ compounds has been considered suitable materials for spintronic devices, and Co₂Cr_{0.6}Fe_{0.4}Al has from then on been the pioneering candidate material.³ The potential of this class has been explored in the context of magneto-resistance applications, such as in giant-magnetoresistance (GMR) and tunnel-magnetoresistance (TMR) devices. Usage as an electrode material for spin injection, where spin polarization is an inevitable prerequisite, and for spintronics applications in general⁴ has been realized. Accompanied by the high Curie temperatures shown by many of the compounds in the Co₂YZ family, the indispensable premises for room-temperature applications are given. On the basis of these premises, TMR ratios of 1900% at low temperatures were accomplished in Co₂MnSi|MgO|Co₂MnSi tunnel junctions by Yamamoto *et al.*⁵ in 2012, whereas the experimental proof of half-metallicity in Co₂MnSi was given by Jourdan *et al.*⁶ just recently. To understand the trends in this class of materials, simple rules have been formed from experimental and theoretical work, and the Slater-Pauling (SP) behavior of these compounds has been intensively studied.⁷⁻⁹

Nowadays, another family of Heusler compounds, the class Mn₂YZ, has attracted considerable attention for implementation as a free magnetic layer in spin-transfer torque devices such as spin-transfer torque random-access memory (STT-MRAM).¹⁰ In these devices, a spin-polarized current is passed through a hard magnetic layer whose magnetization is switched through transfer of angular momentum.¹¹ The most famous member of this group of materials is tetragonal Mn₃Ga.^{12,13} Starting from its prediction as a compensated cubic ferrimagnet, much research in the field has been invested to promote the implementation of this compound. The reasons are

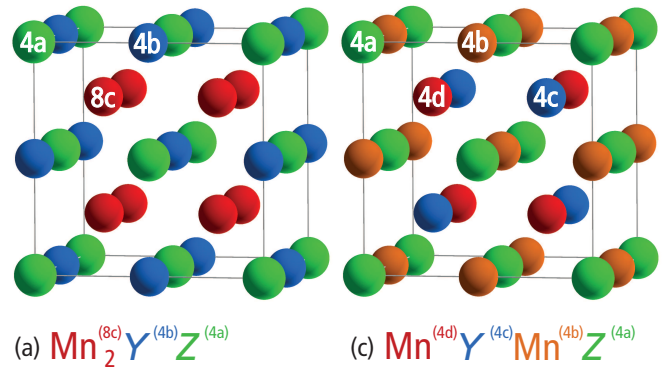


FIG. 1. Two basic ordering possibilities for the ternary X₂YZ composition (X, Y - transition metals and Z - main-group element, marked as red, blue, and green, respectively) within the fcc lattice: (a) L2₁-type: occupation of 8c by X and 4b by Y ("regular" structure); (b) X_a-type: 8c is split into 4c and 4d sites due to their different occupation ("inverse" structure).

found in its properties, namely, a low experimental magnetic moment, high perpendicular magneto-crystalline anisotropy (PMA) owing to its tetragonal structure, and a high Curie temperature of more than 700 K,^{12,14} which ensures the thermal stability of the stored information. These properties, in combination with affordable constituent elements, make this material most attractive for high-technology utilization.

Despite difficulties in the realization of such devices, other members of the Mn₂YZ family have demonstrated their potential.^{10,15} Recently, the spin-gapless semiconductor Mn₂CoAl was predicted and realized, unveiling once again the broad variety of effects to be found in Heusler materials. Peculiar transport properties were expected and have been found in such systems, making them promising candidates for room-temperature semiconductor spintronics.

In addition to the above mentioned materials, the whole family of compounds based on Mn₂YZ may show striking properties. To optimize these materials, we need

a general understanding of how to design compounds with higher spin polarization and achieve compensation of the magnetization in this class. Therefore, we intend to establish guidelines and form simple rules for the Mn_2YZ family of Heusler compounds.

Here we intend to explain the formation of the total moments through monitoring of the local magnetic structure and its influence on easily accessible, measurable properties such as the Curie temperature. While the existence of several Heusler-derived structure types is well known,^{12,16–20} the interplay between the structure, magnetism, and local magnetic moments has not been elucidated as yet, in contrast to the intensively studied cobalt-based Heusler alloys. We will present our work based on theoretical methods, i.e., density functional theory, focusing on the local magnetic structure and the emergence of the magnetic moments on the Mn atoms as the composition is altered. Furthermore, the evaluation of the interatomic exchange in terms of the exchange constant J_{ij} is essential for understanding the formation of the resulting magnetic order. The influence of the electron count on the magnitude of the total moments, the composing local moments, and the exchange interaction is disentangled. In a later publication, we intend to apply the gathered knowledge to tetragonal Mn-based compounds.

II. CRYSTAL AND MAGNETIC STRUCTURES

For ordered cubic Heusler materials, two prototypical structure types exist. The so-called “regular” type (Cu_2MnAl , L2_1 prototype) crystallizes in spacegroup (SG) 225, with three inequivalent Wyckoff positions (8c, 4b, and 4a) incorporating four atoms per unit cell. These positions are occupied according to the following scheme. The 8c Wyckoff position ($\frac{1}{4}, \frac{1}{4}, \frac{1}{4}$) is occupied by two Mn atoms, whereby positions 4b ($\frac{1}{2}, \frac{1}{2}, \frac{1}{2}$) and 4a (0, 0, 0) are filled with Y and Z atoms. Y represents any transition metal (TM) and Z stands for a main group element. The nearest-neighbor coordination can be seen in Fig. 1 (a). Another prototype often appearing in the context of Heusler compounds is the Hg_2CuTi -type structure (sometimes named “inverse” Heusler type), which can be derived from the “regular” Heusler type by interchanging half of the atoms on position 8c with the 4b-position-occupying element. This reduces the symmetry of the cell, leading to spacegroup 216 (X_a -type) with four inequivalent positions in the unit cell. In this case, these are occupied with Mn at 4d ($\frac{1}{4}, \frac{1}{4}, \frac{1}{4}$), Y at 4c ($\frac{3}{4}, \frac{3}{4}, \frac{3}{4}$), Mn at 4b ($\frac{1}{2}, \frac{1}{2}, \frac{1}{2}$), and Z at 4a (0, 0, 0).

The occurrence of these two types of structures for ternary and even quaternary Heusler alloys has been related to a rule of thumb,²¹ which states for X_2YZ that (i) the inversion-symmetric L2_1 -type structure with X occupying site 8c is favored if X has a higher valence electron count than Y. However, (ii) if X is the earlier transition metal, then the structure lacks inversion symmetry, as site 8c splits into two inequivalent sites, 4c and

4d, which are occupied by X and Y, while the second X is found on site 4b. Intermixing of sites has been reported, leading to disordered structural variants of the initial Heusler structure types.²¹ Additional structures in the phase space of Heusler compounds are tetragonal derivatives from the cubic parent phases, which can be obtained from these by elongation or compression of the cell axes.

The family of Mn_2YZ -based Heusler systems is relatively new as compared to other groups such as Co_2YZ , Fe_2YZ , and Ni_2YZ , which have been thoroughly studied over the last few decades. In the context of magnetism, the distinct feature of Mn_2 systems is that their magnetization typically does not exceed $2 \mu_{\text{B}}/\text{f.u.}$ (in certain rare cases it can reach $4 \mu_{\text{B}}$). This is different from the “older” groups, where the magnetization reaches values of 5–6 $\mu_{\text{B}}/\text{f.u.}$ because those materials are known to exhibit ferromagnetic ordering and to incorporate elements with higher number of valence d electrons on the X position (Mn_3Ga : $N_{\text{V}} = 24$, $M = 0 \mu_{\text{B}}$; Co_2MnGa : $N_{\text{V}} = 28$, $M = 4 \mu_{\text{B}}$), leading to a higher magnetization according to the SP rule. The SP rule for four atoms per formula unit describes the relationship between N_{V} of a compound and its measurable magnetic moment, which is given by

$$M = N_{\text{V}} - 24 \quad (1)$$

This kind of behavior was first observed for pure 3d transition metals and alloys by Slater, Pauling, and Friedel,^{22–24} and it was later applied to cubic half-metallic Heusler materials.²⁵ The description and origin of the SP rule for several Heusler materials was given earlier.^{9,21,26} The observable types of magnetic ordering in the Mn_2YZ -based Heusler family will be part of this work and will be explained in the following sections.

III. COMPUTATIONAL DETAILS

The numerical work was carried out within density functional theory as implemented in the all-electron FP-LAPW code, WIEN2K.²⁷ As exchange- and correlation functional, the generalized gradient approximation (GGA) in the parametrization of Perdew, Burke, and Enzerhof was chosen.²⁸ The angular momentum truncation was set to $l_{\text{max}} = 9$ and $RK_{\text{max}} = 9$. The energy convergence criterion was set to 10^{-5} Ry, whereas the charge convergence was set to 10^{-3} Ry. All calculations were carried out on a $20 \times 20 \times 20$ k -mesh, leading to 256 points in the irreducible wedge of the Brillouin zone.

For each compound, calculations starting with ferro- and ferrimagnetic configurations were carried out in space groups No. 225 and 216 according to the regular and inverse Heusler structure types (Fig. 1), respectively. The equilibrium lattice constant was determined through volume relaxations of the unit cell. The results of the calculations for a set of different volumes was fitted to the

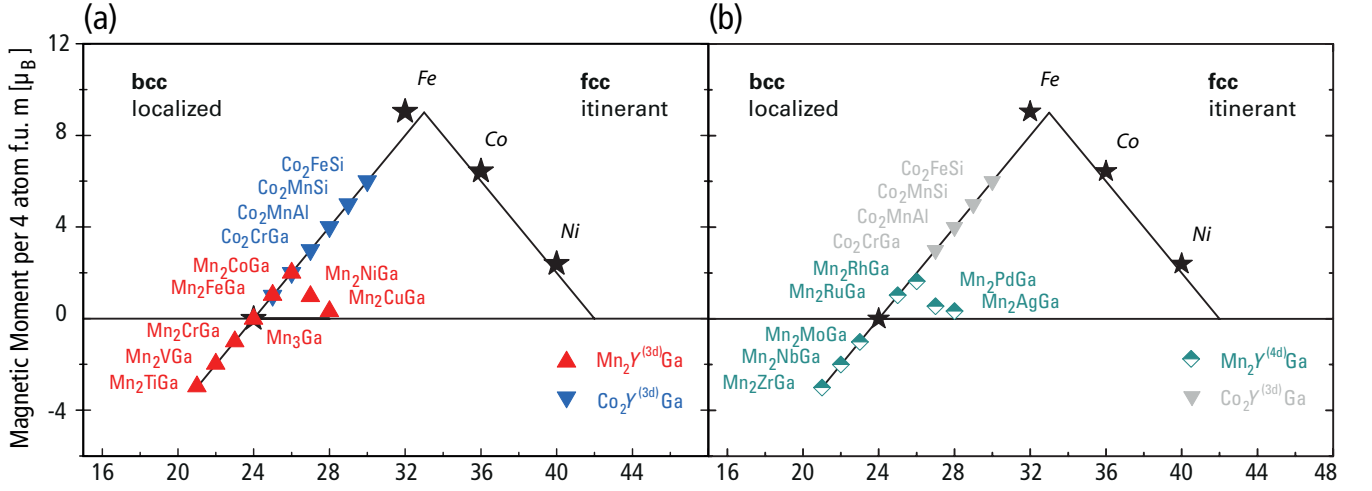


FIG. 2. SP behavior for examples of (a) $\text{Mn}_2\text{Y}^{(3d)}\text{Ga}$ and $\text{Co}_2\text{Y}^{(3d)}\text{Ga}$ compounds and (b) $\text{Mn}_2\text{Y}^{(4d)}\text{Ga}$ compounds.

Birch–Murnaghan equation of state. For some of the presented systems, it is known that the cubic structure is not the global energy minimum and that a tetragonal derivative exists.^{12,29–31} In this stage, these structural instabilities have been ignored deferring an in-depth discussion of these instabilities to an upcoming publication.

IV. RESULTS

A. The Slater–Pauling Rule

The results for the total magnetic moments are shown by means of an SP-curve, which is valid for many of the known Heusler compounds. As seen in Fig. 2, the calculated magnetic moments for each compound in the series $\text{Mn}_2\text{Y}^{(3d)}\text{Ga}$ are well reproduced. For compounds involving Al on the Z position, the values similarly follow the SP rule and are listed in Table I. Even for compounds formed with valence electrons less than $N_V = 24$, SP behavior is observed, although with formally negative magnetic moments. The reason for this is that the minority spin count for $N_V > 24$ is 12, which remains true for $N_V < 24$, albeit with a change of the spin channel, which becomes the majority spin count; this results in the formally negative moments.

For every rule, there are exceptions. For compounds with late transition metals as Y atoms (for Ni and Cu, Pd and Ag, like Pt and Au), the half-metallicity cannot be maintained. Mn_2NiAl and Mn_2NiGa are not half-metallic; however, their magnetic moments are almost integers, and thus these compounds could be mistaken for half-metallic ferromagnets. Also, for Mn_2CuAl , Mn_2CuGa , Mn_2PdGa , Mn_2AgGa , Mn_2PtGa , and Mn_2AuGa , the SP-behavior is no longer valid and the expected moments are smaller than those predicted by the SP rule. The moments decrease and assume non-

integer values, as can be seen in Fig. 2. The reason is explained later in paragraph IV D and Figs. 6 and 8.

B. Structure and Magnetic Ground State

The crystal structures for the Heusler compounds on the SP curve (SPC) occur in two different modifications. For a valence count of $N_V \leq 24$, the L_{21} (SG 255) type is favored, whereas the X_a type (SG 216) is found for $N_V > 24$ (see also Table I, where the results of the structural relaxation are summarized next to the known literature data for both experimental and theoretical studies of cubic alloys, if available). Comparisons with known literature values emphasize the agreement of our work with previous research in the field. Minor discrepancies are usually related to either deviations in the applied theoretical methods and details or to the comparison of high-temperature measurements with zero-temperature ground-state calculations. A disorder-induced decrease of the magnetic moments is also possible.⁴⁴ If the ground-state lattice parameters differ, so do the resulting magnetic moments.

From the rule-of-thumb (Sec.II) and other theoretical work³⁵ on a number of examples, we know that, on the one hand, Mn_2 -based Heusler compounds with early transition elements on the Y position adopt the L_{21} -type structure. On the other hand, compounds involving late transition metals Y adopt the X_a -type inverse Heusler structure. Table I reveals that this kind of behavior is true for all Mn_2 -based Heusler compounds involving 3d TMs on the Y position ($\text{Mn}_2\text{Y}^{(3d)}\text{Ga}$) as well as for the 4d transition metal series ($\text{Mn}_2\text{Y}^{(4d)}\text{Ga}$).

Along with the structural transition, a magnetic transition from parallel to anti-parallel alignment of Mn spins takes place due to Mn occupying site 4b. This begins at the transition point N_V^C , where the magnetization vanishes.³⁶ The type of ferrimagnetic ordering changes

	N_V	SG	a_{opt}	M_{opt}	a_{exp}	M_{exp}	Ref.	a_{theo}	M_{theo}	Ref.
Mn ₂ TiAl	21	225	5.96	-2.98				5.96	-2.98	32
Mn ₂ VAl	22	225	5.81	-2.00	5.92	-1.94	33, 34	5.80	-2.00	35
Mn ₂ CrAl	23	225	5.73	-1.04				5.71	-1.00	35
Mn ₃ Al	24	225	5.80	0.00				5.80	0.00	36
Mn ₂ FeAl	25	216	5.76	1.00				5.73	1.01	35
Mn ₂ CoAl	26	216	5.74	2.00	5.80	2.00	15	5.75	2.00	35
Mn ₂ NiAl	27	216	5.81	1.19				5.64	1.44	31
Mn ₂ CuAl	28	216	5.90	0.20	5.91	0.22	37	5.85	0.22	38
Mn ₂ TiGa	21	225	5.95	-2.97				5.95	2.98	32
Mn ₂ VGa	22	225	5.82	-1.98	6.10	-1.66	33			
Mn ₂ CrGa	23	225	5.76	-1.00				5.71	-1.00	39
Mn ₃ Ga	24	225	5.82	0.01			12	5.82	0.01	36
Mn ₂ FeGa	25	216	5.76	1.03			29	5.80	1.05	40
Mn ₂ CoGa	26	216	5.78	2.00				5.86		41
Mn ₂ NiGa	27	216	5.85	1.18	5.91		42		1.28	42
Mn ₂ CuGa	28	216	5.94	0.33				5.94	0.33	43
Mn ₂ ZrGa	21	225	6.14	-3.00						
Mn ₂ NbGa	22	225	6.00	-2.00						
Mn ₂ MoGa	23	225	5.91	-1.01						
Mn ₂ RuGa	25	216	5.96	1.03	6.00	1.15	44			
Mn ₂ RhGa	26	216	5.98	1.64						
Mn ₂ PdGa	27	216	6.12	0.55						
Mn ₂ AgGa	28	216	6.22	0.34						

TABLE I. Numerically optimized lattice parameters a_{opt} and magnetization M_{opt} of Mn₂-based Heusler alloys compared to the experimental (a_{exp} , M_{exp}) and theoretical (a_{theo} , M_{theo}) literature data.

and becomes more complex, as will be pointed out in the following section.

C. Stability Considerations and Heats of Formation

For estimating the stability of the investigated compounds, the heats of formation were calculated from the elemental crystals in their ground-state modification (except for Mn, where an anti-ferromagnetic bcc structure was used as an approximation) using total energy differences. Fig. 3 shows the changes in the approximated formation energy within the series of compounds under study. One sees that the compounds are stable within the range of -100 to -180 kJ/mol, except for Mn₂AgGa. The existence of some compounds such as Mn₂CoGa⁴⁵ is experimentally proven through synthesis. Nevertheless, phases incorporating the investigated stoichiometries may exist in other crystal structures, such as the tetragonal derivatives of cubic Heusler structures. These findings will be presented in a later publication.

Consideration of the total energy difference between the inverse and regular structures $\Delta E_{216-225} = E_{216} - E_{225}$ for the given chemical composition X_2YZ (Fig. 4), confirms that the $4b$ site is going to be occupied by the earlier transition metal among Mn and Y. This leads to the formation of the regular structures for the $Y=\text{Ti, V, Cr, Zr, Nb, Mo}$ and inverse structures for the $Y=\text{Fe, Co, Ni, Cu, Ru, Rh, Pd}$ and Ag containing Heusler materials. The total energy

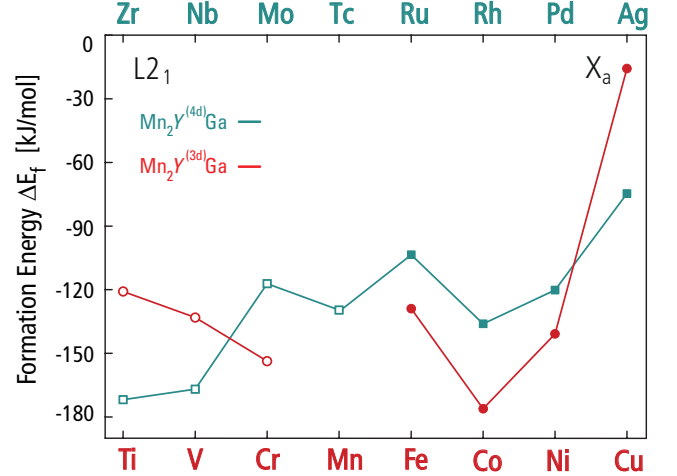


FIG. 3. Formation energies estimated at $T = 0$ for Mn₂Y^(3d)Ga and Mn₂Y^(4d)Ga compounds, as initial guess regarding the stability of these compounds. Open symbols denote the L2₁-type structure. Filled symbols denote the X_a-type structure.

difference can be interpreted as site-preference energy for the interchange of Mn and Y that distinguishes both structure types. For instance, in Mn₂CrGa, with a rather small site-preference energy, indicating that the *regular* type structure is not strongly preferred, thermally induced disorder is more likely to occur than

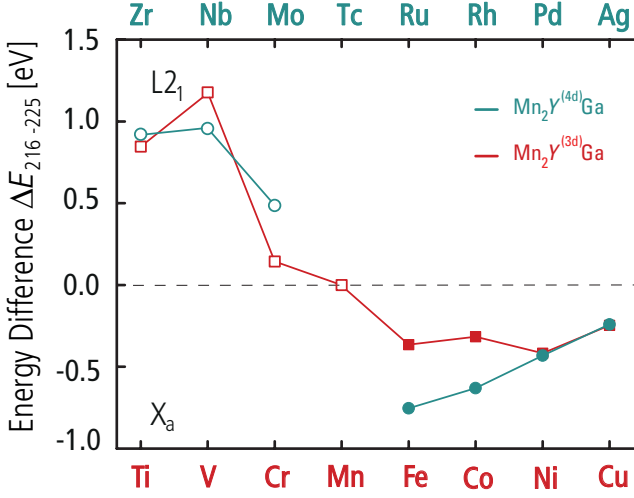


FIG. 4. Total energy difference between the inverse and regular structures $\Delta E_{216-225} = E_{216} - E_{225}$ calculated for $\text{Mn}_2\text{Y}^{(3d)}\text{Ga}$ and $\text{Mn}_2\text{Y}^{(4d)}\text{Ga}$ cubic Heusler materials.

for example for Mn_2CoGa and Mn_2VGa , with solid energy differences. Additional information about the stability of the phases under investigation was obtained from the densities of state (DOS) that are discussed in detail in the following section. It has proven useful to look for sharp peaks in the DOS at the Fermi edge that are symptoms of instabilities in the system. This applies to Mn_2FeGa ²⁹ and Mn_3Ga ,¹² which have been experimentally realized in the tetragonal inverse structure. It is known that besides Mn_2FeGa and Mn_3Ga there are tetragonal phases for the 3d transition metals (TMs) involving Mn-based compounds, such as Mn_3Al , and Mn_2NiGa . Furthermore, we could show that tetragonal alloys may exist in the series involving late TMs of the IV period. A detailed discussion of these phases shall be postponed to a later publication; we emphasise, however, that possible tetragonal derivatives from cubic Heusler phases do not prove their existence, as other relaxation mechanisms such as disorder phenomena may minimize the total energy. Nevertheless, the instabilities do give a strong hint, as has been seen in *ab-initio* studies related to shape-memory compounds.

D. Electronic Structure

The calculations reveal that nearly all compounds are at least pseudo-half-metallic or even truly half-metallic with the associated gap in the *minority* densities of state (DOS) for compounds with a valence electron count of less than 24 and a gap in the *majority* DOS for more than 24 electrons. It is worth mentioning that the definition of spin-up and spin-down electrons is connected with the choice of the magnetic moment as positive. However, we may allow negative values to emphasize the occupancy of

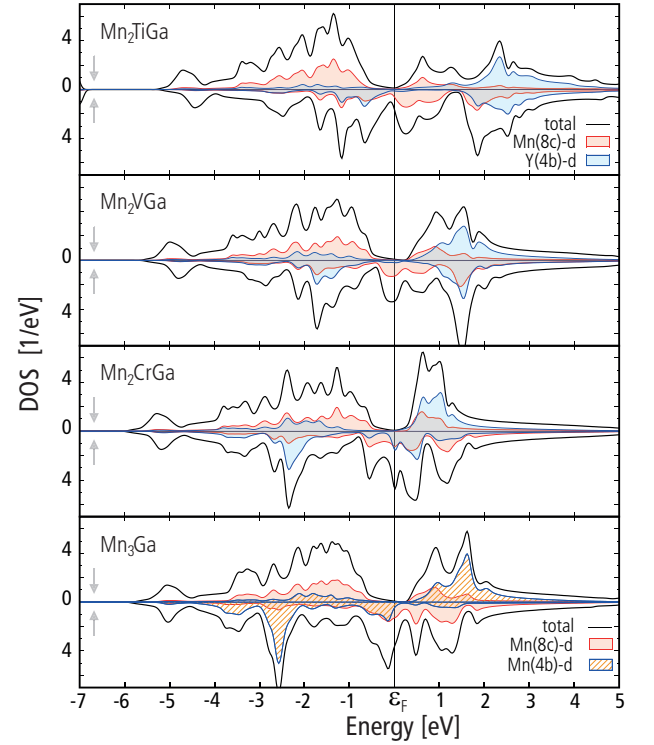


FIG. 5. Densities of states of the $\text{Mn}_2\text{Y}^{(3d)}\text{Ga}$ compounds with $\text{Y}=\text{Ti}, \text{V}, \text{Cr}, \text{Mn}$.

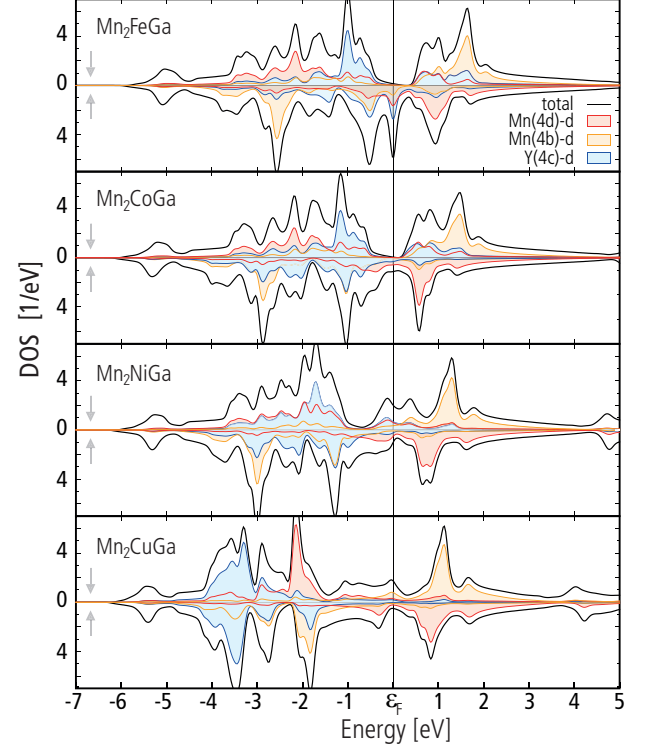


FIG. 6. Densities of states of the $\text{Mn}_2\text{Y}^{(3d)}\text{Ga}$ compounds with $\text{Y}=\text{Fe}, \text{Co}, \text{Ni}, \text{Cu}$.

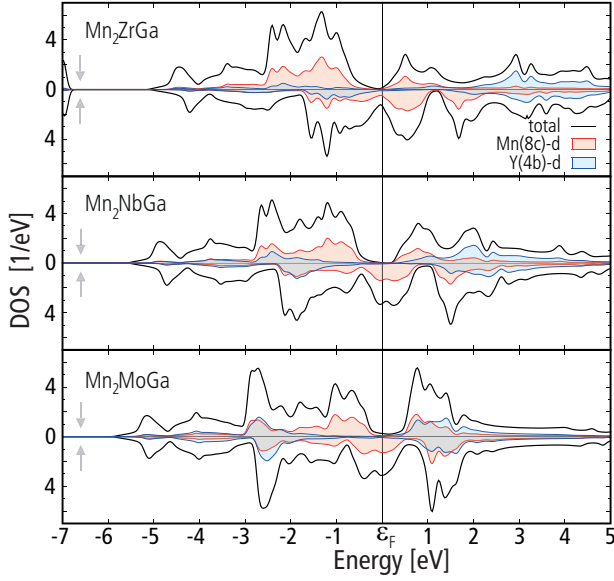


FIG. 7. Densities of states of the $\text{Mn}_2\text{Y}^{(4d)}\text{Ga}$ compounds with $\text{Y}=\text{Zr}, \text{Nb}, \text{Mo}$.

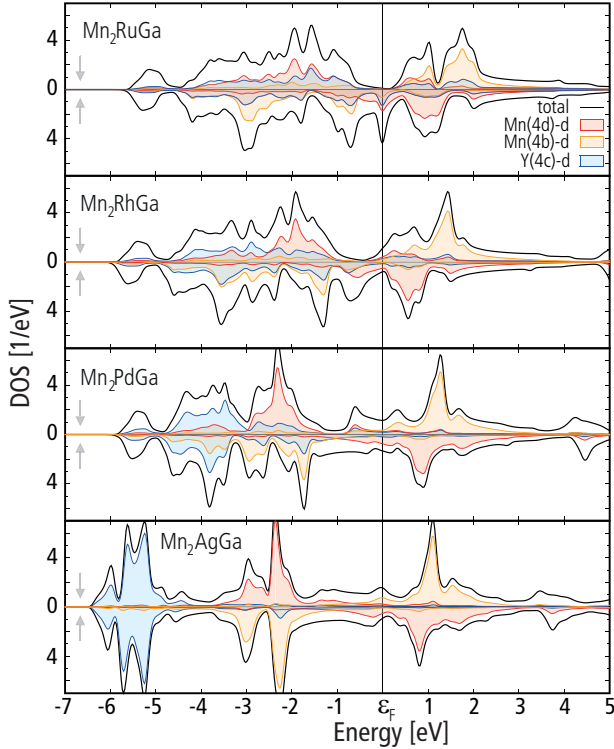


FIG. 8. Densities of states of the $\text{Mn}_2\text{Y}^{(4d)}\text{Ga}$ compounds with $\text{Y}=\text{Ru}, \text{Rh}, \text{Pd}, \text{Ag}$.

the d -states according to the SP rule, although the notion of negative moments is unphysical. Still doing so leads to a better understanding of the mechanism of magnetic ordering. Although Figs. 5 and 6 were chosen to exhibit the gap in the spin-down channel for all compounds, the minority channel changes from the spin-down state to the

spin-up state as the electron count crosses 24 electrons per formula unit.

N_V	$N_{V,Y}$	$\text{Mn}_2\text{Y}^{(3d)}\text{Ga}$	$P/\%$	$\text{Mn}_2\text{Y}^{(4d)}\text{Ga}$	$P/\%$
21	4	Mn_2TiGa	83	Mn_2ZrGa	82
22	5	Mn_2VGa	94	Mn_2NbGa	98
23	6	Mn_2CrGa	97	Mn_2MoGa	85
24	7	Mn_3Ga	96		
25	8	Mn_2FeGa	95	Mn_2RuGa	95
26	9	Mn_2CoGa	93	Mn_2RhGa	15
27	10	Mn_2NiGa	35	Mn_2PdGa	7
28	11	Mn_2CuGa	53	Mn_2AgGa	24

TABLE II. The total number of the valence electrons, N_V and valence electrons of the Y atom, $N_{V,Y}$, and the calculated spin polarization, P , of the DOS at the Fermi edge of the $\text{Mn}_2\text{Y}^{(3d)}\text{Ga}$ and $\text{Mn}_2\text{Y}^{(4d)}\text{Ga}$ series.

In Figs. 5 and 6, the DOS for both structure types are compared. A feature seen in the DOS is that the gap at the Fermi energy is bordered by Mn states for the L2₁-type structure, whereas this is not the case for the inverse compounds. A second property is the prominent downward trend of the Y d -states. Independent of the structure type, the local environment of Mn exhibits tetrahedral symmetry, which leads to the SP curve being continuous across the transition point at $N_V = 24$, leaving the near-half metallic behavior unchanged. Following Ouardi and Galankis,^{9,46} the gap in the minority channel in Mn_2 -based alloys is the result of hybridization of the X atoms on site 8c in the SG 225, which are again tetrahedrally coordinated with their neighboring atoms. The final size of the gap is determined by the crystal field splitting of the e_g and t_{2g} states (at the Γ point), which is determined by the symmetry and coordination of the Mn atoms.

The DOS for Mn_2NiGa and Mn_2CuGa explains the deviation from the SP curve because the gap at the Fermi energy closes. This is so because the d -electron states of Ni and Cu disappear from the Fermi energy being drawn into the core. The states at the Fermi edge are now mainly composed of s electrons for Mn_2AgGa . Condensing this finding into one number that is closely connected with the concept of half-metallicity, the spin polarization, P , emphasizes the preceding facts and is listed for the investigated compounds in Table II. Once more, the failure of the SP rule for compounds with more than 26 valence electrons is apparent in terms of the spin polarization.

E. Local Magnetic Moments

A truly large number of publications on the SP behavior of various compounds exists,^{7,26,47} and yet the local magnetic structure has not been intensively investigated so far, even though the local magnetic structure is closely related with the magnetic phenomenon. First-principles calculations are a sophisticated tool to access site-resolved quantities such as local magnetic moments,

even though the partitioning of a solid into atomic regions is an arbitrary procedure and approximate projection techniques need to be applied in most cases. But as experimental information on atomic magnetic moments in bulk Heusler materials is rather incomplete, we focus our attention on the local magnetic and electronic environment of the Mn atoms in both structure types. We show that the magnetic moment in inverse Heusler compounds (X_a) of one Mn atom is locked at about $3 \mu_B$, whereas no such rule is found for the local moments of the Mn-based L_{21} -type compounds, where Mn occupies the tetrahedrally coordinated position $8c$.

To see this, the local magnetic moments of the $Mn_2Y^{(3d)}Ga$ and $Mn_2Y^{(4d)}Ga$ compounds are shown in Fig. 9, which in panels c and d provides a schematic overview of the type of magnetic order. The left-hand side of the plots Fig. 9 (a, b) for $N_V < 24$ regime displays the local moments of the transition metal atoms in the L_{21} structure. The electron count increases through the variation of the Y atom occupation from Y=Ti to Cu and from Y=Zr to Ag. As the electron count is increased by one, the magnetic moments of the systems, following the SP curve, increase by $1 \mu_B$. Considering the series $Mn_2Y^{(3d)}Ga$, we recognize that the moments of Y($4b$) and Mn($8c$) display almost linear behavior. On the other hand, as the magnetic moment on Y($4b$) increases, the absolute value of Mn($8c$) decreases for both series with a change of slope at the Cr position. Increasing the electron count therefore leads to a filling of either the minority channel ($N_V \leq 24$) or the majority channel ($N_V \geq 24$).

TABLE III. Atomic magnetic moments in $Mn_2Y^{(3d)}Ga$ Heusler compounds; M is the total magnetization.

regular	N_V	a_{opt}	Mn($8c$)	–	Y($4b$)	Z($4a$)	M
Mn_2TiGa	21	5.95	-1.87		0.62	0.05	-2.97
Mn_2VGa	22	5.82	-1.45		0.84	0.02	-1.98
Mn_2CrGa	23	5.76	-1.16		1.27	0.00	-1.00
Mn_3Ga	24	5.82	-1.53		3.02	0.04	0.01
inverse	N_V	a_{opt}	Mn($4d$)	Y($4c$)	Mn($4b$)	Z($4a$)	M
Mn_2FeGa	25	5.76	-1.97	0.21	2.78	0.01	1.03
Mn_2CoGa	26	5.78	-1.81	1.00	2.85	-0.01	2.00
Mn_2NiGa	27	5.85	-2.38	0.34	3.17	0.01	1.18
Mn_2CuGa	28	5.94	-2.81	0.04	3.11	0.00	0.33

TABLE IV. Atomic magnetic moments in $Mn_2Y^{(4d)}Ga$ Heusler compounds; M is the total magnetization.

regular	N_V	a_{opt}	Mn($8c$)	–	Y($4b$)	Z($4a$)	M
Mn_2ZrGa	21	6.14	-1.76		0.33	0.07	-3.00
Mn_2NbGa	22	6.00	-1.23		0.36	0.03	-2.00
Mn_2MoGa	23	5.91	-0.69		0.30	0.02	-1.01
inverse	N_V	a_{opt}	Mn($4d$)	Y($4c$)	Mn($4b$)	Z($4a$)	M
Mn_2RuGa	25	5.96	-2.29	0.07	3.16	0.03	1.03
Mn_2RhGa	26	5.98	-2.20	0.31	3.42	0.03	1.64
Mn_2PdGa	27	6.12	-3.23	0.08	3.64	0.02	0.55
Mn_2AgGa	28	6.22	-3.31	0.04	3.60	0.01	0.34

As shown in section IV D, every compound is at least nearly half-metallic, reflecting the change of the moments by means of the site-resolved densities of state (Fig. 5). The decreasing number of states in the minority channel and the increasing number of states in the majority channel for both Mn and Y atoms are related to the change in the local moments. Filling states of Y and Mn atoms at the same time, where the Mn magnetic moment is aligned anti-parallel to the Y atom and is consequently decreasing. The trends of the L_{21} Mn-based Heusler compounds intriguingly resemble the nature of the local moments in Co_2 -based Heusler compounds.⁸

Moving forward in the series, perhaps the most outstanding Heusler alloy, Mn_3Ga , marks the transition point between both cubic structure types. Although Mn_3Ga is found to adopt the L_{21} structure in the cubic approximation, it exhibits properties of the inverse Heusler structure, namely, the anti-parallel alignment of Mn atoms on sites $4d$ and $4b$. The determining characteristic property of Mn-based inverse Heusler compounds clearly is this antiparallel alignment. This is displayed in Fig. 9. Through its peculiar behavior, Mn_3Ga is not only an exceptional compound of the L_{21} series, but it also constitutes the *transition point* between both structure types. Additionally, the total magnetic moment for Mn_3Ga is supposed to vanish,³⁶ as it marks the *compensation point*, following the SP rule as well. It is emphasized again that tetragonal Heusler compounds were not considered for this part of the study, and it is noted again that Mn_3Ga does not exhibit a cubic structure; as with Mn_3Al , Mn_2FeGa , Mn_2NiGa , and Mn_2NiAl , Mn_3Ga has been found to be tetragonal.

With Mn occupying the $4b$ site, the local moment on site $4d$ increases in absolute value. But most important, the local magnetic moment of Mn on site $4b$ is locked at $3 \mu_B$. Although some compounds are known in the literature, a comprehensive overview of the local magnetic structure has not been provided yet. Therefore, the remarkable consistency of the moment on site $4b$ has not been appreciated enough.

Beyond the transition point, the magnetic ordering, following the crystallographic ordering, changes from parallel to antiparallel alignment of the Mn spins. Owing to a symmetry reduction of index t_2 (*translationengleiche* subgroup), the Wyckoff position $8c$ splits into $4d$ and $4c$, which are now occupied by Mn($4d$) and Y($4c$), the second Mn atom now occupying site $4b$, which is electronically distinct from site $4d$. The electric potential experienced on the Mn sites is different owing to the nearest neighbors, i.e. Mn($4d$) is coordinated by four Ga($4a$) and four Mn($4b$) atoms, whereas Mn($4b$) is surrounded by four Mn($4d$) and four Y($4c$) atoms. One observes that the nearest-neighbor combination, Mn($4b$)–Y($4c$), results in a high local moment on Mn($4b$) and ferromagnetic coupling of both species, whereas the Mn($4b$)–Mn($4d$) coupling is antiferromagnetic, as in the elemental crystal.

While varying the $Y^{(4d)}$ atoms, the Y atom d states decrease in energy and act as charge sinks, leading to

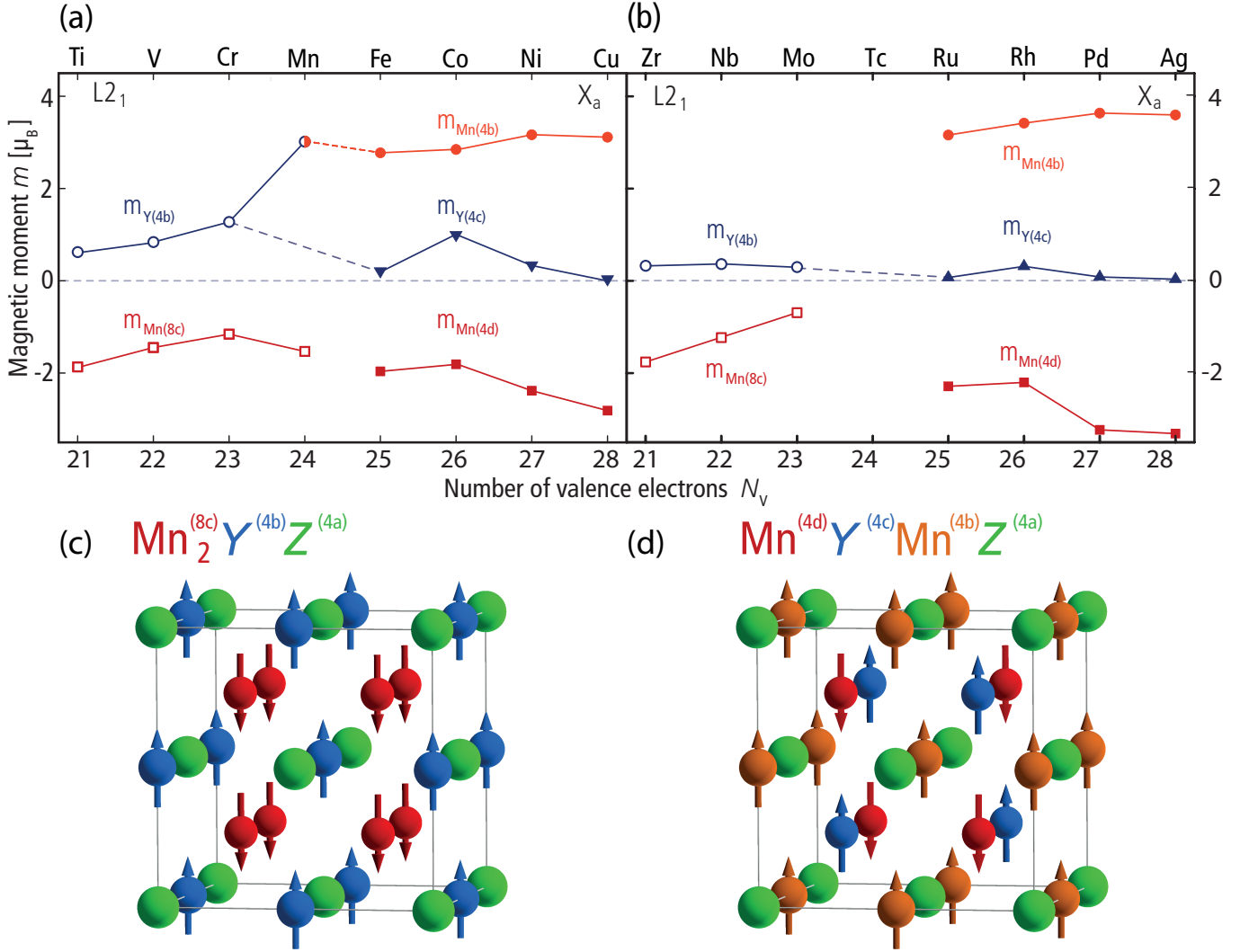


FIG. 9. Atomic magnetic moments in (a) $\text{Mn}_2\text{Y}^{(3d)}\text{Ga}$ and (b) $\text{Mn}_2\text{Y}^{(4d)}\text{Ga}$ -compounds. Open symbols denote the $L2_1$ -type structure. Filled symbols denote the X_a -type structure. Panels (c) and (d) show the magnetic ordering corresponding to the $L2_1$ and X_a types, respectively.

an increase of the magnetic moment on the Mn(4d) position owing to its atomic states and chemical environment. The character of the Y atom d state is therefore reflected in the energy levels of the Heusler compounds. This behavior of the magnetic moments with increasing electron count is demonstrated in Fig. 9.

The compounds shown on the right-hand side of Figures 9 (a,b) are composed by the data for the inverse compounds, and thus the contributions to the change of the total magnetic moment stem from the Mn atoms on position 4d only. Meanwhile, the change in the local moments of the Y atoms is significant for Co only, whereas Fe, Ni, and Cu carry small moments that do not follow a particular trend.

Furthermore, the Mn-based Heusler compounds incorporating transition metals from the IV period are studied in the same fashion. In contrast to the series involving 3d transition metals, the magnetic moments are largely built

by the Mn atoms only. The contribution of the transition metals is of minor importance. As for the lighter homologues, the SP behavior breaks down for alloys with 27 or more valence electrons. The local magnetic moments almost compensate, as the transition metals on position 4c (Pd, Ag) do not contribute to the total moment.

F. Exchange Coupling and Curie Temperatures

The interaction of the magnetic moments is typically parametrized using the effective Heisenberg Hamiltonian, where the interaction strength is described by the so-called exchange constants or pair interaction energies J_{ij} : $H = -\sum_{ij} J_{ij} \hat{e}_i \hat{e}_j$, where $\hat{e}_{i,j}$ are the directional unit vectors along the magnetic moments on sites i and j . Knowing the set of $\{J_{ij}\}$, one can estimate the magnetic order (positive J corresponds to the parallel coupling,

negative - to the antiparallel one) and the ordering temperature (we will call it the Curie temperature T_C also in case of a ferrimagnet). The proper way to calculate T_C is via the exact T -dependent solutions of the parametrized Heisenberg model using Monte-Carlo simulations. In the present study, we are more interested in general trends, rather than in exact solutions; therefore we will use the standard mean-field approximation⁴⁸ (MFA), for which $k_B T_C = 2/3 \cdot J_{\max}$, where J_{\max} is the maximal eigenvalue of the $\{J_0^{\mu\nu}\}$ matrix, with $J_0^{\mu\nu} = \sum_{j \in \{\nu\}} J_{0j}$, where 0 and j are the site indices, 0 - is fixed within the μ sublattice, j - runs over the ν sublattice. In this case, $J_0^{\mu\nu}$ represents the effective interaction of the 0-th site from the sublattice μ with the whole sublattice ν . The sum over ν sites is supposed to be infinite; in practice it is truncated at a sufficiently large cluster radius, typically a few lattice constants. For the calculation of J_{ij} pair interactions we use the real-space Liechtenstein approach,⁴⁸ which assumes that the magnetic moments and the band structure do not change when the directions of the moments are varied. These calculations are carried out using the Munich SPR-KKR Green's function based method.⁴⁹ Combined with the MFA, we usually obtain a slightly overestimated T_C .

In addition, we will use another complimentary formalism, the so-called spherical approximation (SPA) proposed by Moriya.⁵⁰ In the SPA the exchange interactions are obtained in reciprocal space as $J_{\nu\mu}(\mathbf{k})$, where ν and μ designate sublattice-types. For each \mathbf{k} in the Brillouin zone all eigenvalues of the matrix $J_{\nu\mu}(\mathbf{k})$ are obtained, calling them $j_{n,\mathbf{k}}$. Then T_C is estimated by means of

$$k_B T_C = \frac{2}{3} M_{\text{tot}}^2 \left[\sum_{n,\mathbf{k}} j_{n,\mathbf{k}}^{-1} \right]^{-1},$$

where M_{tot}^2 is the sum of the squared local moments.^{7,51} In contrast to the Liechtenstein formalism, this approach accounts for the change of the size of the magnetic moments upon their rotations. In practice it is found to give slightly underestimated values of T_C . The list of calculated T_C is summarized in Table V.

Since the differences between magnetic moments in iso-electronic Mn_2YZ with $Z=\text{Al}$ and Ga are rather small (Tab. V), we will restrict further discussion to the set of Mn_2YGa compounds only. Both MFA and SPA estimations of the Curie temperatures are compared in Fig. 10. It follows, despite the noticeable difference, the general trends shown by both approaches are rather similar: with increasing N_V the T_C decreases (very slightly in case of MFA and more noticeably in case of SPA for $Y^{(3d)}$) for the regular compounds ($N_V < 24$), and then significantly increases for the inverse compounds ($N_V > 24$). Such behavior to a large extent is defined by the nearest (between the $4b$ and $4c/4d$ sites) and next-nearest neighbor exchange coupling constants. Here we do not plot them explicitly, but since the dominant contribution is contained in the effective sublattice coupling $J_0^{\mu\nu}$ Figure 11 gives an idea how the magnetic order is formed.

TABLE V. The Curie temperatures of $\text{Mn}_2Y^{(3d)}\text{Ga}$, $\text{Mn}_2Y^{(3d)}\text{Al}$ and $\text{Mn}_2Y^{(4d)}\text{Ga}$ Heusler compounds. Present calculations using MFA and SPA formalisms are referred as $T_{C,\text{MFA}}$ and $T_{C,\text{SPA}}$; the values from the literature $T_{C,\text{lit}}$ are marked by the subscripts “ t ” or “ e ”, which refer to theoretical calculations and experimental measurements, respectively.

Material	$T_{C,\text{MFA}}$ [K]	$T_{C,\text{SPA}}$ [K]	$T_{C,\text{lit}}$ [K]	Ref.
Mn_2TiGa	557	525	663 _t	32
Mn_2VGa	587	387	783 _e	52
Mn_2CrGa	578	213		
Mn_3Ga	221	314	482 _t	53
Mn_2FeGa	601	322		
Mn_2CoGa	928	668	710 _e , 886 _t	45, 41
Mn_2NiGa	1005	586	600 _e	54
Mn_2CuGa	1491	954		
Mn_2ZrGa	207	185		
Mn_2NbGa	289	239		
Mn_2MoGa	140	81		
Mn_2RuGa	619	369	560 _e	44
Mn_2RhGa	576	408		
Mn_2PdGa	809	490		
Mn_2AgGa	1240	751		
Mn_2TiAl	428		665	32
Mn_2VAl	588		663 _t , 638 _t , 760 _e	52, 53, 55
Mn_2CrAl	549			
Mn_3Al	306	342		
Mn_2FeAl	614	200		
Mn_2CoAl	985	740	720 _e , 890 _t	15, 41
Mn_2NiAl	1140	452		
Mn_2CuAl	1539	884		

For $N_V < 24$ regime the nearest neighbors of Mn which sits in $8c$ ($4c/4d$) are the weakly- or nonmagnetic elements in $4b$, i.e. $Y=\text{Ti}$, V and Cr . The corresponding nearest-neighbor exchange coupling constants (estimated from the Liechtenstein approach) are $J \approx -7$, -9.8 and -11.7 meV, respectively. Despite that most of the Mn-Mn next-neighbor interactions ($4c-4d$, $4d-4d$, etc.) are also antiparallel, the dominating nearest Y -Mn antiparallel interaction typically fixes the ferromagnetic order in $\text{Mn}(8c)$ sublattice, set by the indirect $\text{Mn}(8c)$ - $Y(4b)$ - $\text{Mn}(8c)$ coupling.⁵⁵ Thus, the relatively low Curie temperatures for $N_V < 24$ can be understood as a result of the relatively strong degree of magnetic frustration (i.e., the presence of the competing interactions). This becomes especially evident in case of Mn_2CrGa ($N_V = 23$) and Mn_3Ga ($N_V = 24$) which show the lowest $T_C \approx 200$ K within both the SPA and the MFA. The fact, that magnetic frustration is just another side of electronic instability is clearly seen in the density of states, which exhibits peaks at the Fermi energy for both compounds. Furthermore, in spite of the frustration in the group of inverse compounds ($N_V > 24$) being lower, there are still a few unstable materials, such as Mn_2FeGa and Mn_2RuGa : the first one is known to be tetragonal,¹⁰ the second one relaxes through chemical disorder.⁴⁴ By increasing the number of valence electrons in the $N_V > 24$ regime the cubic structure becomes more stable. Thus,

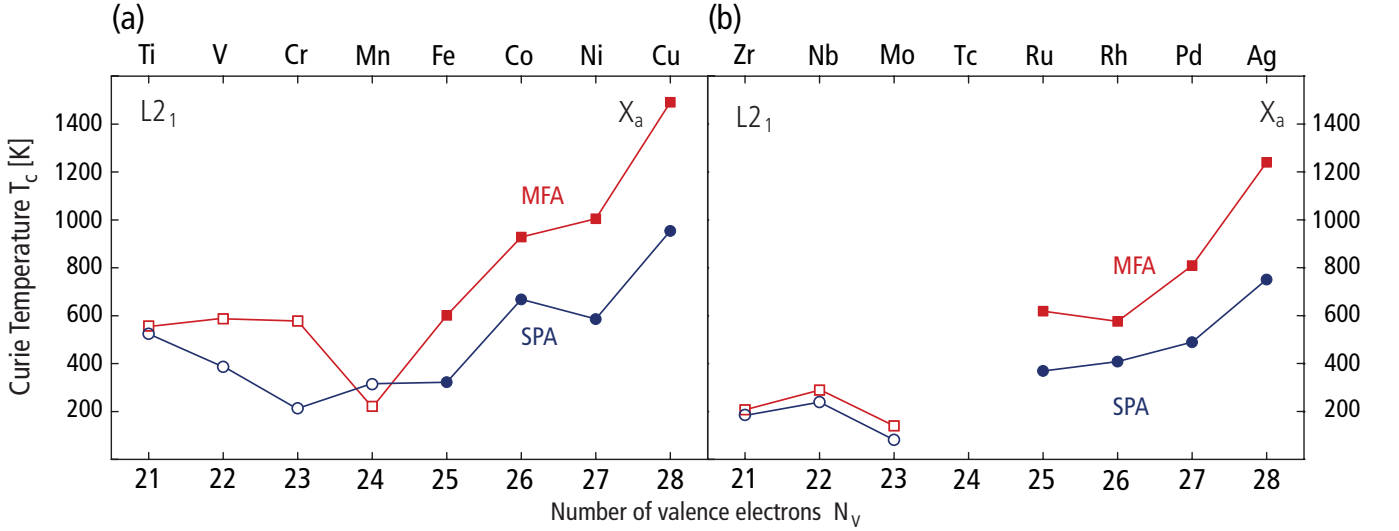


FIG. 10. The calculated Curie temperatures of the Heusler compounds containing Ga. The results of the mean-field approximation (MFA) is compared with that of the spherical approximation (SPA). Open symbols: L2₁-type structure. Filled symbols: X_a-type structure.

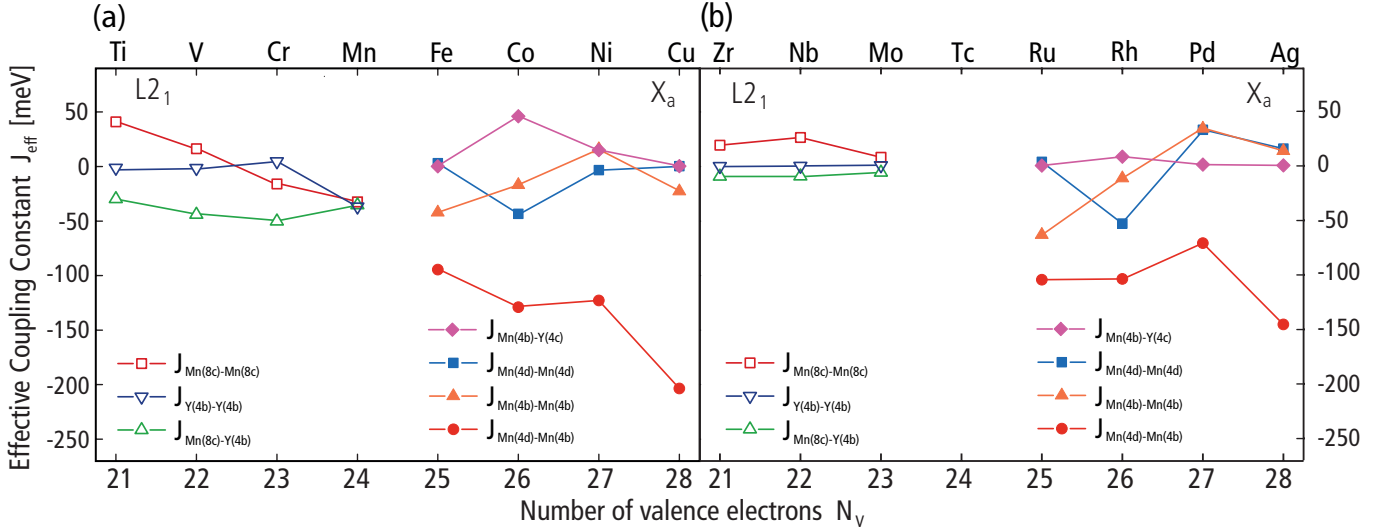


FIG. 11. Effective exchange coupling constants $J_0^{\mu\nu} = \sum_{j \in \nu} J_{0j}$ for the $\text{Mn}_2\text{Y}^{(3d)}\text{Ga}$ and $\text{Mn}_2\text{Y}^{(4d)}\text{Ga}$ compounds. Open symbols: L2₁-type structure. Filled symbols: X_a-type structure.

T_C increases for Co, Ni and Cu containing compounds. An important aspect within the inverse group is that the exchange coupling constants between nearest-neighbors, i.e. between Mn in 4b and Mn in 4c, become very large: -20.1 , -29.7 , -33.2 and -40.2 meV for Fe, Co, Ni and Cu containing materials, respectively. As we see, a similar situation is observed for $\text{Y}^{(4d)}$ containing group as well.

V. SUMMARY

The SP curves show that the magnetic moments of Mn-based compounds, independent of the structure type, are continuous across the compensation point and follow the SP rule (with the exception of compounds with $N_V \geq 27$). The total magnetization M is composed of contributions of different characters (localized or itinerant) for the different structure types (Figs. 9 and 11). Considering the empirical rules regarding the chemical ordering (Sec. II) and accounting for the trends in the local moments, we can understand how the magnetization in Mn_2YZ systems is formed. The L2₁-type Heusler

compounds are purely itinerant ferrimagnets with small magnetic moments on the Mn atoms that are coupled ferromagnetically. The Y atoms on 4b sites are of minor importance in the sum of the various contributions to the total moment. They are coupled antiparallel to the Mn moments on the 8c sites. The magnetism in the X_a -type (inverse) Heusler compounds is composed of a large, localized^{2,56} system-independent moment on Mn(4b) of about $3 \mu_B$. The magnetic moment of Mn(4d) increases in absolute value, whereas the Y atoms, with the exception of Co, contribute small moments in both structure types. Even for the compounds that do not follow the SP rule (Mn₂NiGa, Mn₂CuGa, Mn₂RuGa, Mn₂RhGa, Mn₂PdGa), the trends regarding the local moments are still valid. Regarding the large constant localized moment, Mn is thus the only 3d transition metal element in inverse Heusler compounds that behaves like a rare-earth element.

The calculated exchange constants supply Curie temperatures in two different approximations that are likely to border the experimental values. Fig. 10 can be separated into the L2₁ and X_a parts. In L2₁, the Curie temperatures show only little variation. Starting with the

materials with $N_V = 24$ (X_a transition point), care has to be taken with these values because of the occurrence of a phase change to tetragonal structures for some compounds. If the compounds remain in the cubic structure, the trend shown indicates an increase in the Curie temperature owing to the increase of the local moments and an increase in the exchange constants. The latter can be attributed to the increase in conduction electron concentration, which is the essence of the Zener–DeGennes^{57,58} exchange model for ferromagnetic metals. We believe the antiferromagnetic coupling of the nearest-neighbor Mn atoms is an atomic property of Mn in the elementary metal.

ACKNOWLEDGMENTS

The authors gratefully acknowledge financial support from Project P 1.2-A of research unit FOR 1464 “AS-PIMATT”) and the European Research Council (ERC) “Idea Heusler!”.

-
- ¹ R. A. de Groot, F. M. Mueller, P. G. van Engen, and K. H. J. Buschow, Phys. Rev. Lett. **50**, 2024 (Jun 1983)
 - ² J. Kübler, A. R. Williams, and C. B. Sommers, Phys. Rev. B **28**, 1745 (1983)
 - ³ T. Block, C. Felser, G. Jakob, J. Ensling, B. Mühling, P. Gülich, and R. J. Cava, J. Solid State Chem. **176**, 646 (2003)
 - ⁴ C. Felser and G. H. Fecher, *Spintronics: From Materials to Devices* (Springer Berlin Heidelberg, 2013)
 - ⁵ H. Liu, Y. Honda, T. Taira, K. Matsuda, M. Arita, T. Uemura, and M. Yamamoto, Appl. Phys. Lett. **101**, 132418 (2012)
 - ⁶ M. Jourdan, J. Minár, J. Braun, A. Kronenberg, S. Chadov, B. Balke, A. Gloskovskii, M. Kolbe, H. J. Elmers, G. Schönhense, H. Ebert, C. Felser, and M. Kläui, Nat. Commun. **5** (2014)
 - ⁷ J. Kübler, G. H. Fecher, and C. Felser, Phys. Rev. B **76**, 024414 (2007)
 - ⁸ H. C. Kandpal, G. Fecher, and C. Felser, J. Phys. D: Appl. Phys. **40**, 1507 (2007)
 - ⁹ I. Galanakis, P. H. Dederichs, and N. Papanikolaou, Phys. Rev. B **66**, 174429 (2002)
 - ¹⁰ J. Winterlik, S. Chadov, A. Gupta, V. Alijani, T. Gasi, K. Filsinger, B. Balke, G. H. Fecher, C. A. Jenkins, F. Casper, J. Kübler, G.-D. Liu, L. Gao, S. S. P. Parkin, and C. Felser, Adv. Materials **24**, 6283 (2012)
 - ¹¹ J. Slonczewski, J. Magn. Magn. Materials **159**, L1 (1996)
 - ¹² B. Balke, G. H. Fecher, J. Winterlik, and C. Felser, Appl. Phys. Lett. **90**, 152504 (2007)
 - ¹³ F. Wu, S. Mizukami, D. Watanabe, H. Naganuma, M. Oogane, Y. Ando, and T. Miyazaki, Appl. Phys. Lett. **94** (2009)
 - ¹⁴ J. Winterlik, B. Balke, G. H. Fecher, C. Felser, M. C. M. Alves, F. Bernardi, and J. Morais, Phys. Rev. B **77**, 054406 (2008)
 - ¹⁵ S. Ouardi, G. H. Fecher, C. Felser, and J. Kübler, Phys. Rev. Lett. **110**, 100401 (2013)
 - ¹⁶ J. Sticht, K.-H. Höck, and J. Kübler, J. Phys.: Condens. Matter **1**, 8155 (1989)
 - ¹⁷ E. Krén and G. Kádár, Solid State Commun. **8**, 1653 (1970)
 - ¹⁸ H. Niida, T. Hori, and Y. Nakagawa, J. Phys. Soc. Japan **52**, 1512 (1983)
 - ¹⁹ H. Kurt, K. Rode, M. Venkatesan, P. S. Stamenov, and J. M. D. Coey, Phys. Rev. B **83**, 020405 (Jan 2011)
 - ²⁰ H. Kurt, N. Baadji, K. Rode, M. Venkatesan, P. S. Stamenov, S. Sanvito, and J. M. D. Coey, Appl. Phys. Lett. **101**, 132410 (2012)
 - ²¹ T. Graf, C. Felser, and S. S. P. Parkin, Progress in Solid State Chemistry **39**, 1 (2011)
 - ²² J. C. Slater, Phys. Rev. **49**, 931 (1936)
 - ²³ L. Pauling, Phys. Rev. **54**, 899 (1938)
 - ²⁴ J. Friedel, Il Nuovo Cim. **7**, 287 (1958)
 - ²⁵ J. Kübler, Physica B+C **127**, 257 (1984)
 - ²⁶ S. Skaftouros, K. Ozdogan, E. Sasioglu, and I. Galanakis, Phys. Rev. B **87**, 024420 (Jan 2013)
 - ²⁷ P. Blaha, K. Schwarz, G. K. H. Madsen, D. Kvasnicka, and J. Luitz, **WIEN2k, An Augmented Plane Wave + Local Orbitals Program for Calculating Crystal Properties** (Karlheinz Schwarz, Techn. Universität Wien, Austria, 2001)
 - ²⁸ J. P. Perdew, K. Burke, and M. Ernzerhof, Phys. Rev. Lett. **77**, 3865 (1996)
 - ²⁹ T. Gasi, A. K. Nayak, J. Winterlik, V. Ksenofontov, P. Adler, M. Nicklas, and C. Felser, Appl. Phys. Lett. **102**, 202402 (2013)
 - ³⁰ G. D. Liu, J. L. Chen, Z. H. Liu, X. F. Dai, G. H. Wu, B. Zhang, and X. X. Zhang, Appl. Phys. Lett. **87**, 262504 (2005)

- ³¹ H. Luo, G. Liu, F. Meng, S. Li, W. Zhu, G. Wu, X. Zhu, and C. Jiang, *Physica B* **405**, 3092 (2010)
- ³² M. Meinert, J. Schmalhorst, and G. Reiss, *J. Phys.: Condens. Matter* **23**, 036001 (2011)
- ³³ K. H. J. Buschow and P. G. van Engen, *J. Magn. Magn. Materials* **25**, 90 (1981)
- ³⁴ C. Jiang, M. Venkatesan, and J. M. D. Coey, *Solid State Commun.* **118**, 513 (2001)
- ³⁵ H. Luo, Z. Zhu, L. Ma, S. Xu, X. Zhu, C. Jiang, H. Xu, and G. Wu, *J. Phys. D: Appl. Phys.* **41**, 055010 (2008)
- ³⁶ S. Wurmehl, H. C. Kandpal, G. H. Fecher, and C. Felser, *J. Phys.: Condens. Matter* **18**, 6171 (2006)
- ³⁷ Z. Q. Feng, H. Z. Luo, Y. X. Wang, Y. X. Li, W. Zhu, G. H. Wu, and F. B. Meng, *Phys. Stat. Sol. (a)* **207**, 1481 (2010)
- ³⁸ S. T. Li, Z. Ren, X. H. Zhang, and C. M. Cao, *Physica B* **404**, 1965 (2009)
- ³⁹ H. Luo, Z. Zhu, G. Liu, S. Xu, G. Wu, H. Liu, J. Qu, and Y. Li, *J. Magn. Magn. Materials* **320**, 421 (2008)
- ⁴⁰ H. Z. Luo, H. W. Zhang, Z. Y. Zhu, L. Ma, S. F. Xu, G. H. Wu, X. X. Zhu, C. B. Jiang, and H. B. Xu, *J. Appl. Physics* **103**, 083908 (2008)
- ⁴¹ M. Meinert, J.-M. Schmalhorst, and G. Reiss, *J. Phys.: Condens. Matter* **23**, 116005 (2011)
- ⁴² G. D. Liu, X. F. Dai, S. Y. Yu, Z. Y. Zhu, J. L. Chen, G. H. Wu, H. Zhu, and J. Q. Xiao, *Phys. Rev. B* **74**, 054435 (2006)
- ⁴³ A. Chakrabarti, M. Siewert, T. Roy, K. Mondal, A. Banerjee, M. E. Gruner, and P. Entel, *Phys. Rev. B* **88**, 174116 (Nov 2013)
- ⁴⁴ T. Hori, M. Akimitsu, H. Miki, K. Ohoyama, and Y. Yamaguchi, *Appl. Phys. A* **74**, 737 (2002)
- ⁴⁵ G. J. Li, E. K. Liu, H. G. Zhang, J. F. Qian, H. W. Zhang, J. L. Chen, W. H. Wang, and G. H. Wu, *Appl. Phys. Lett.* **101**, 102402 (2012)
- ⁴⁶ S. Ouardi, G. H. Fecher, B. Balke, A. Beleanu, X. Kozina, G. Stryganyuk, C. Felser, W. Klöß, H. Schrader, F. Bernardi, J. Morais, E. Ikenaga, Y. Yamashita, S. Ueda, and K. Kobayashi, *Phys. Rev. B* **84**, 155122 (Oct 2011)
- ⁴⁷ I. Galanakis and P. H. Dederichs, in *Half-metallic Alloys*, Lecture Notes in Physics, Vol. 676, edited by I. Galanakis and P. Dederichs (Springer Berlin Heidelberg, 2005) pp. 1–39
- ⁴⁸ A. I. Liechtenstein, M. I. Katsnelson, P. V. Antropov, and A. V. Gubanov, *J. Magn. Magn. Materials* **67**, 65 (1987)
- ⁴⁹ H. Ebert, D. Ködderitzsch, and J. Minár, *Rep. Prog. Phys.* **74**, 096501 (2011)
- ⁵⁰ T. Moriya, *Spin fluctuations in itinerant electron magnetism*, Springer Series in Solid-State Sciences No. 56 (Springer Berlin Heidelberg, 1985)
- ⁵¹ J. Kübler, *Theory of Itinerant Electron Magnetism, Ch.5* (Oxford University Press, New York, 2009)
- ⁵² K. R. Kumar, J. A. Chelvane, G. Mark, G. Markandeyulu, S. K. Malik, and N. H. Kumar, *Solid State Commun.* **150**, 70 (2010)
- ⁵³ J. Kübler, *J. Phys.: Condens. Matter* **18**, 9795 (2006)
- ⁵⁴ C. G. F. Blum, S. Ouardi, G. H. Fecher, B. Balke, X. Kozina, G. Stryganyuk, S. Ueda, K. Kobayashi, C. Felser, S. Wurmehl, and B. Büchner, *Appl. Phys. Lett.* **98**, 252501 (2011)
- ⁵⁵ E. Sasioglu, L. M. Sandratskii, and P. Bruno, *J. Phys.: Condens. Matter* **17**, 995 (2005)
- ⁵⁶ M. Meinert, J.-M. Schmalhorst, C. Klewe, G. Reiss, E. Arenholz, T. Böhnert, and K. Nielsch, *Phys. Rev. B* **84**, 132405 (Oct 2011)
- ⁵⁷ C. Zener, *Phys. Rev.* **82**, 403 (1951)
- ⁵⁸ P. G. de Gennes, *Phys. Rev.* **118**, 141 (1960)